EUROfusion

EUROFUSION CP(15)06/06

L. Buehler et al.

Theoretical Studies of MHD Flows in Support to HCLL Design Activities

12th International Symposium on Fusion Nuclear Technology (ISFNT)
Jeju Island, Korea
(14th September 2015 – 18th September 2015)

This work has been carried out within the framework of the EUROfusion Consortium and has received funding from the Euratom research and training programme 2014-2018 under grant agreement No 633053. The views and opinions expressed herein do not necessarily reflect those of the European Commission.

Theoretical studies of MHD flows in support to HCLL design activities

L. Bühler, C. Mistrangelo
Karlsruhe Institute of Technology, Postfach 3640, 76021 Karlsruhe, Germany

Abstract

Theoretical studies are performed to predict magnetohydrodynamic flow pattern and pressure drop in typical geometric components of the liquid metal manifold for a HCLL blanket module. The interaction of the flow with the strong magnetic field that confines the fusion plasma is analyzed by asymptotic techniques and by numerical simulations. The flows in feeding and draining manifolds are electrically coupled to each other via leakage currents which may cross the common wall that hydraulically separates both channels. This results in complex flow paths in the manifold and in additional pressure drop.

Key words: HCLL blanket, magnetohydrodynamics (MHD), liquid metal manifolds, asymptotic analysis, numerical simulations
PACS:

1. Introduction

In support of design activities for a helium cooled lead lithium (HCLL) blanket module for a DEMO reactor [1] and for development of the liquid metal ancillary system it is necessary to estimate pressure losses caused by electromagnetic forces. The latter ones are due to the interaction of the electrically conducting liquid breeder lead lithium (PbLi) with the magnetic field that confines the fusion plasma. Previous experimental and theoretical analyses of magnetohydrodynamic (MHD) flows in simplified HCLL blanket geometries suggest that the major fraction of pressure drop arises in the distributing manifold [2]. Even if velocity and pressure drop in single breeder units are small they may become much larger in the manifold, since it has to feed and drain up to 8 breeder units. Moreover, the geometry of the manifold is quite complex as can be seen in Fig.1. Before entering the breeding zone the PbLi follows a tortuous path, since the manifold is periodically changing its cross-section. In addition, ducts are partly occupied by the helium distributing chambers. As a result 3D current loops are induced that lead to significant 3D MHD effects with associated additional pressure losses. The latter ones have to be determined by appropriate experiments and by numerical simulations for developing a reliable design of a HCLL blanket module and for predicting its operating conditions and performance.

In order to support ongoing design activities and to get an overview of MHD phenomena in manifolds of a HCLL blanket a numerical study is performed to simulate flow conditions in typical geometric components of a manifold. Pressure distribution and occurrence of flow recirculation are investigated. Results depend on the position and conductivity of the wall that separates distributing and collecting manifolds and on the electromagnetic flow coupling between neighboring fluid regions.

2. Problem description

In the following we consider MHD flows in a generic model geometry which has typical features of the liquid metal manifold foreseen in a HCLL blanket module [1] (see Fig.1). The geometry is shown in Fig.2. It consists of two ducts which are

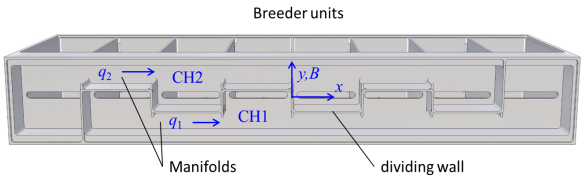

Fig. 1. MHD test section for studying the pressure drop in one PbLi manifold of a HCLL blanket module.

electrically connected across a step-shaped dividing wall. As a result the flow undergoes periodic expansions and contractions and due to the electromagnetic coupling at the common separating wall the flow in one duct influences the one in the neighboring channel. The overall dimensions of the cross section are $4a$ and $2a$ in magnetic field direction y and in transverse direction z, respectively, where the Hartmann length a is used to define later the nondimensional parameters. The half-length of one period in axial direction x is L and the alternating position of the dividing wall measured from the middle of the manifold is $\pm\Delta y$. In the limiting case when $\Delta y = 0$ we have two electrically coupled straight square channels. In general the flow rates q_1 and q_2 in the two ducts may differ, depending on applied pressure differences.

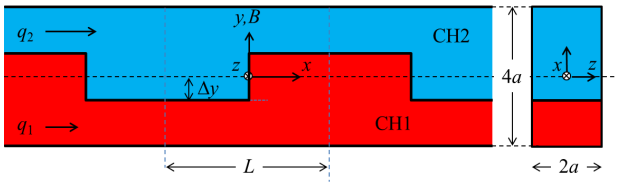

Fig. 2. Sketch of a generic manifold geometry. Two ducts with expansions and contractions are electrically coupled at a step-shape dividing wall.

3. Mathematical formulation

In the following coordinates are scaled by the Hartmann length a. Inertialess pressure driven MHD flows, as considered in the present study, are governed by the non-dimensional Navier-Stokes equation and by mass conservation

$$\nabla p = \frac{1}{Ha^2}\nabla^2\mathbf{v} + \mathbf{j}\times\mathbf{B},\ \nabla\cdot\mathbf{v} = 0, \qquad (1)$$

where p, $\mathbf{v}$, and $\mathbf{B}$ denote pressure, velocity and magnetic field scaled by $\sigma a u_0 B^2$, u_0 and B, respectively. As a characteristic velocity we choose the average value in both ducts, i.e. $u_0 = (q_1 + q_2)\,/\,(8a^2)$.

The electric current density $\mathbf{j}$ is determined by the dimensionless Ohm's law and conservation of charge

$$\mathbf{j} = -\nabla\phi + \mathbf{v}\times\mathbf{B},\ \nabla\cdot\mathbf{j} = 0, \qquad (2)$$

where $\mathbf{j}$ stands for current density normalized by $\sigma u_0 B$ and ϕ represents the electric potential scaled by $a u_0 B$.

The dimensionless parameter in (1) is the Hartmann number

$$Ha = aB\sqrt{\frac{\sigma}{\rho\nu}},$$

which quantifies the relative importance of electromagnetic forces to viscous forces. The inertialess assumption is justified if the interaction parameter is very high, $N = \sigma a B^2/(\rho u_0) \to \infty$, when electromagnetic forces dominate over inertia forces. The physical properties of the liquid metal, the density ρ, electric conductivity σ and kinematic viscosity ν are assumed to be constant.

When the flow is inertialess and periodic, it is sufficient to consider only a representative part of length L as shown in Fig. 2 with given inlet and exit pressure values for each channel. Periodicity implies that at $x = \pm L/2$ velocity and potential do not change along the axial direction, $\partial\mathbf{v}/\partial x = 0$, $\partial\phi/\partial x = 0$. At the fluid wall interface the flow satisfies the no-slip condition, $\mathbf{v} = 0$. Since the wall thickness t_w is much smaller than a we may apply the thin-wall condition to describe closure of currents along duct walls,

$$\frac{\partial\phi}{\partial n} = \nabla_w\cdot(c\nabla_w\phi), \quad \text{where} \quad c = \frac{t_w\sigma_w}{a\sigma} \qquad (3)$$

is the wall conductance parameter and ∇_w stands for the gradient in the plane of the wall [3]. Both ducts are electrically coupled at the common dividing wall where we have $\phi_1 = \phi_2$.

For strong magnetic fields, i.e. for $Ha \gg 1$ viscous effects are confined to very thin boundary layers while the core of the flow behaves practically as being inviscid. This property is exploited by applying an inviscid core-flow analysis for the solution of equations (1)-(3) with viscous boundary layer correction at the walls [4]. In this code sudden expansions and contractions are approximated by continuous but steep transitions. In addition complete numerical simulations for inertial MHD flows are performed using a numerical code based on the open source package OpenFOAM [5]. A more realistic geometry close to the one shown in Fig.1 with walls of finite thickness and conductivity is considered.

4. Results

4.1. *Asymptotic analysis*

In the following, results will be shown first for a reference case with nondimensional length $l = L/a = 4$, which is close to the geometry proposed in [1]. As reference expansion ratio we choose $\Delta y = 0.5$, which is close to the one foreseen in the design ($\Delta y = 0.64$). As a result of the assumed equal pressure differences in the two channels, $\Delta p_1 = \Delta p_2$, both flow rates become equal as well, $q_1 = q_2$. The wall conductance parameter has been chosen as $c = 0.1$ and results are presented for $Ha = 1000$. The electric potential is plotted in Fig.3 on the surface of the channels. In the narrow parts of the ducts the velocity is larger. This yields higher values of induced potential on the side walls at $z = \pm 1$ (see dark red areas). Where the cross sections are larger the magnitude of induced potential difference remains smaller.

3D effects at expansions and contractions lead to modifications in the velocity distribution compared to fully developed conditions. This can be seen in subplots of Fig.3 where profiles of axial velocity component u are displayed at several axial positions. The profile at $x = -1.59$ corresponds to almost fully developed conditions with core velocities of the order one and the well known side layer jets along walls parallel to the magnetic field. At $x = -0.2$, shortly before the expansion of CH1 (contraction of CH2), we observe already significant modifications in the side layers of CH2 where now a fraction of flow moves in reversed direction. Immediately behind the expansion of CH1 (contraction of CH2) at $x = 0.2$ the highest velocities are observed in CH2 and a partly reserved flow occurs in the layers of CH1. Further downstream at $x = 1.59$ we observe again almost fully developed conditions with highest jet velocity in CH2.

In the small parts of the ducts the induced currents are large and as a result we find here the strongest pressure gradients. This can be seen in Fig. 4, e.g. for CH1 in the regions $-2 < x < 0$ and $4 < x < 6$ or for CH2 in the range $0 < x < 4$. Near the expansions and contractions the magnitude of pressure gradients is further increased due to additional Lorentz forces caused by 3D electric currents as explained in [6] or in [7]. In the small channels where the velocities are high, mechanical energy is transformed into electrical energy, transferred via the conducting walls to the neighboring larger ducts

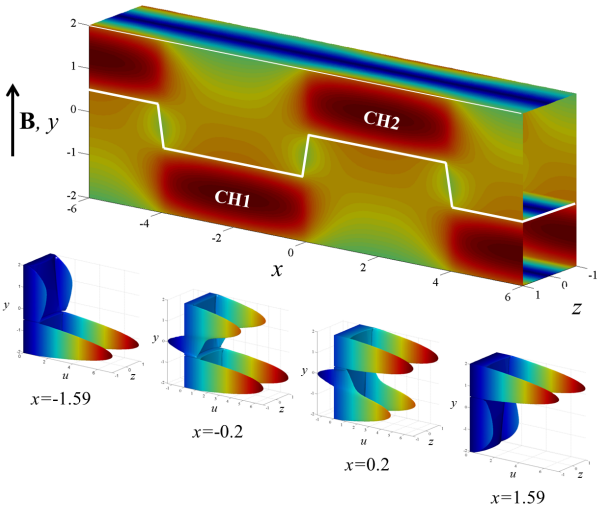

Fig. 3. Magnitude of surface potential plotted on the walls of the ducts for $c = 0.1$, $Ha = 1000$, $\Delta p_1 = \Delta p_2$, and profiles of axial velocity at different axial positions.

and released there partly as mechanical energy to drive the slower flow in the larger cross section. The small ducts act as local electric MHD generators while the larger ducts function as electromagnetic pumps. This can be seen by the increasing pressure with respect to the mean value when moving along the streamwise direction in CH1 in the range $0 < x < 4$ and for CH2 in the regions $-2 < x < 0$ and $4 < x < 6$.

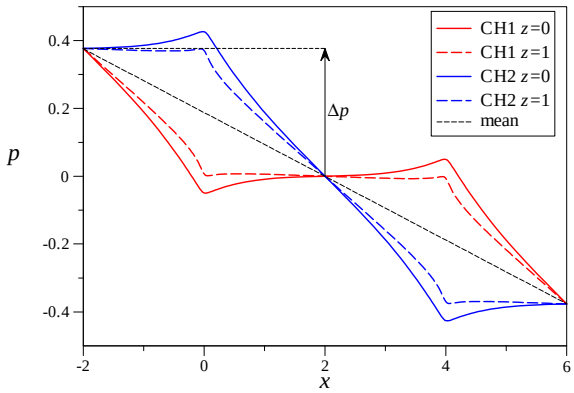

Fig. 4. Pressure along a full length of a period, plotted along a center line at $z = 0$ and along a line near the side wall at $z = 1$ for channels CH1 and CH2.

The pressure drop Δp over a half length of a period as indicated in Fig.4 has been investigated by a parametric study for different expansion ratios Δy. Results are shown in Fig.5. For $\Delta y = 0$ we observe the pressure drop of a fully developed flow in two straight, electrically coupled channels

of length $l = 4$. With increasing Δy the pressure drop increases for two reasons. First the flow has to pass through smaller cross sections. This leads to increased velocity and higher pressure drop. On the other hand, larger expansion ratios increase the intensity of 3D MHD effects associated with additional pressure drop [6]. For small Δy the additional pressure drop appears moderate but already at $\Delta y = 0.6$, which is still a bit smaller than that in the blanket, the increase in Δp is already 91% compared to a flow in two parallel channels.

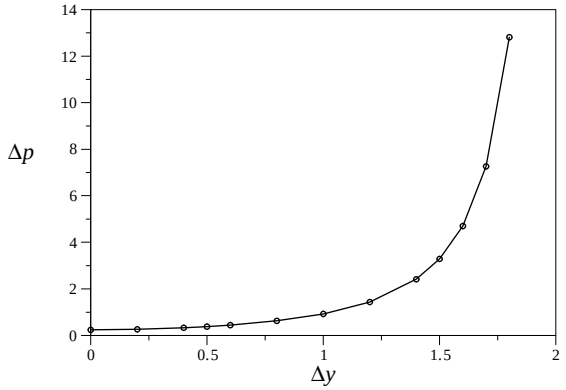

Fig. 5. Pressure drop Δp along half of a period as a function of the expansion ratio Δy.

Finally, it is worth to mention that in the real manifold the flow rates in CH1 and CH2 differ, depending on the axial positions along the manifold since CH1 feeds the breeder units while CH2 collects the flow from the breeder zone. This leads to different pressure drops in both channels of the manifold. To get an impression how pressure drops and flow rates are related to each other a parametric study has been performed in which the ratio of applied pressure differences is varied in a wide range. Fig.6 shows the flow rates in CH1 and CH2 as a function of the pressure ratio $\Delta p_1/\Delta p_2$ between both ducts. For $\Delta p_1/\Delta p_2 = 1$ we observe equal flow rates in both channels as a result of perfect symmetry of the problem. When Δp_1 is increased compared to Δp_2 the flow rate q_1 increases and q_2 decreases. For vanishing Δp_2, i.e. for $\Delta p_1/\Delta p_2 \to \infty$ both flow rates approach finite asymptotic limiting values which are indicated at the right border of Fig.6. There remains a finite flow rate in CH2 even if the pressure drop in this channel vanishes. The reason for this is the electromagnetic coupling according to which the flow is driven by the energy supplied from CH1. Same reasoning holds for $\Delta p_1/\Delta p_2 \to 0$.

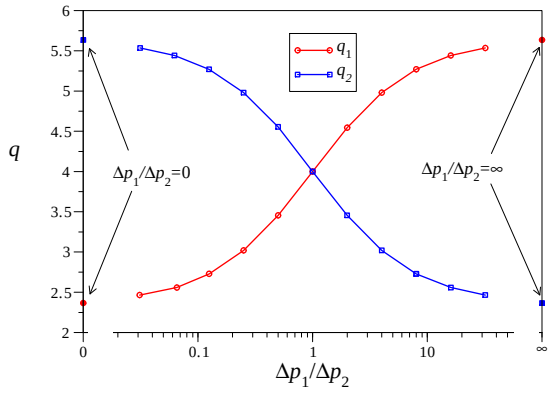

Fig. 6. Flow rates q_1 and q_2 depending on the pressure ratio $\Delta p_1/\Delta p_2$ in both ducts.

It has been shown that in the extreme case a finite flow rate exists in CH2 even if $\Delta p_2 = 0$. The structure of this flow can be observed in two cross sections shown in Fig. 7. At $x = -1.59$ we observe relatively high side wall jets in CH1 and a core velocity larger than one. Due to electromagnetic coupling the flow in CH1 pulls that in the core of CH2 in same direction. This leads to a build up of pressure along the axial direction that drives the backward oriented jets in CH2 as shown in Fig. 8. In the region $0 < x < 4$ the pressure gradients in both channels point in same direction and as a result here the side walls jets have same streamwise orientation.

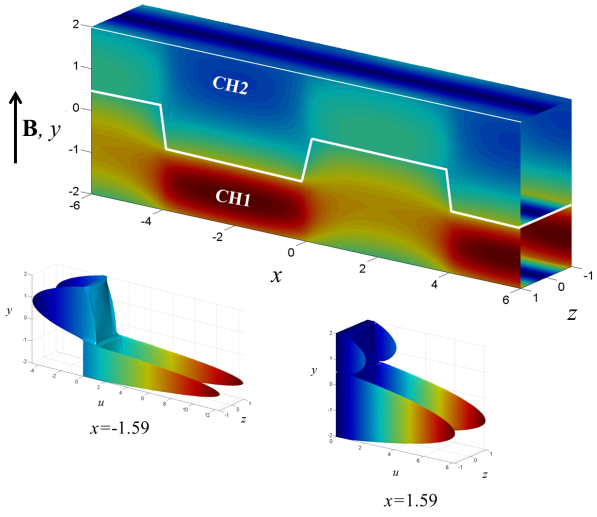

Fig. 7. Magnitude of surface potential plotted on the walls of the ducts for $c = 0.1$, $Ha = 1000$, $\Delta p_2 = 0$ and profiles of axial velocity at different axial positions.

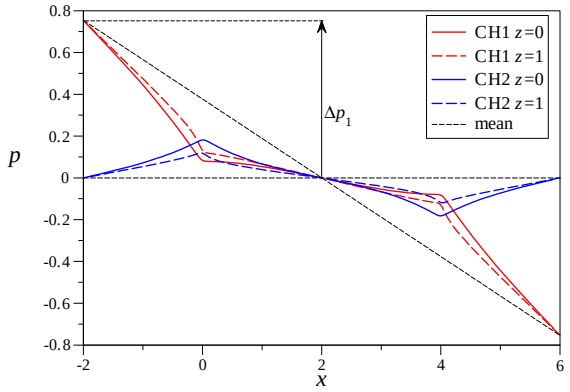

Fig. 8. Pressure along a full length of a period, plotted along a center line at $z = 0$ and along a line near the side wall at $z = 1$ for channels CH1 and CH2 when $\Delta p_2 = 0$.

4.2. *Numerical simulations*

While results shown so far have been obtained for a model geometry using an inertialess asymptotic theory and assuming that the walls are very thin, the real geometry has walls of finite thickness and inertia effects could have an influence on pressure drop [8]. This is studied by ongoing 3D numerical simulations where the geometry is modelled with more details and with the real finite wall thickness. In these simulation all boundary layers are well resolved with finer grid spacing near the walls. In total 9 millions of grid points have been used inside the fluid domain and about 11 millions inside the solid structure. First results have been obtained and one example is shown in Fig.9, where contours of electric potential are plotted on the fluid-wall interface. A qualitative comparison with results obtained with the asymptotic theory (Fig.3) shows that the simple model geometry provides reasonable solutions.

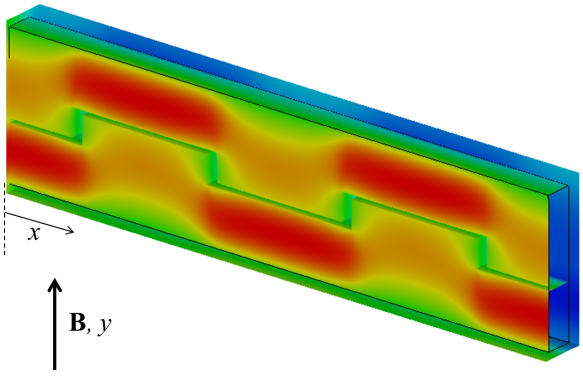

Fig. 9. Contours of potential plotted on the fluid-wall interface of the ducts for $Ha = 1000$, $N = 1000$, $\Delta p_1 = \Delta p_2$.

The axial distribution of pressure obtained by the 3D numerical simulations is displayed in Fig.10 and Fig.11. The contours presented in Fig.10 show only deviations from an assumed mean linear pressure distribution $p = -kx$ for a better visualization of 3D effects near expansions and contractions. The variation of pressure in CH1 and CH2 along the red and blue lines indicated in Fig.10 can be seen in Fig.10. We observe here the same behavior as in our model geometry with steeper gradients in narrow channels and pressure recovery in larger ducts, compared to mean linear pressure distribution. The magnitude of pressure drop is larger than in previous model calculations since the walls here are much thicker and better conducting.

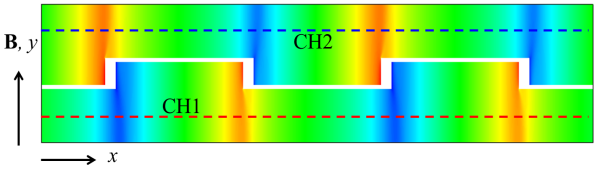

Fig. 10. Conturs of pressure deviations from a mean linear distribution $p = -k$ at $z = 0$ for $Ha = 1000$, $N = 1000$, $\Delta p_1 = \Delta p_2$.

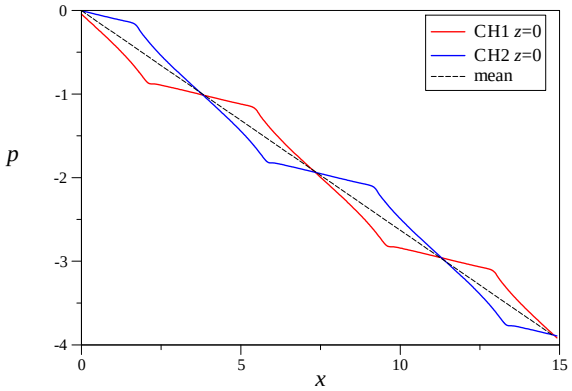

Fig. 11. Pressure along two periods, plotted along a center line at $z = 0$. Results are obtained by numerical simulation for realistic HCLL geometry (without helium manifolds).

5. Conclusions

Basic MHD phenomena in a model geometry for a HCLL manifold have been investigated by an asymptotic analysis of 3D flows in electrically coupled domains and by numerical simulations. It has been found that electromagnetic flow coupling across the common wall that divides the manifold

in two sub-channels has a strong influence on flow distribution and pressure drop. Mechanical energy lost in smaller channels by large pressure drops is transfered via leakage currents to the larger ducts where partial pressure recovery is observed. Nevertheless, due to Joule dissipation in 3D current loops, a significant fraction of flow energy is dissipated which increases the mean pressure drop along the manifold. Periodic expansions and contractions of similar size, as foreseen in the design of the HCLL blanket module for a DEMO reactor, may lead to an increase of pressure drop by more than 90% compared to flows in straight ducts.

First 3D numerical simulations have been performed which confirm the results obtained by the asymptotic analysis. Further numerical studies are ongoing for investigation of inertia effects. The influence of partial blocking of PbLi channels by the helium manifolds will be also analyzed in future studies.

Acknowledgment: This work has been carried out within the framework of the EUROfusion Consortium and has received funding from the Euratom research and training programme 2014-2018 under grant agreement No 633053. The views and opinions expressed herein do not necessarily reflect those of the European Commission.

References

[1] G. Aiello, J. Aubert, N. Jonqures, A. L. Puma, A. Morin, G. Rampal, Development of the helium cooled lithium lead blanket for DEMO, Fusion Engineering and Design 89 (7-8) (2014) 1444–1450.

[2] C. Mistrangelo, L. Bühler, MHD mock-up experiments for studying pressure distribution in a helium cooled liquid-metal blanket, IEEE Transactions on Plasma Science 38 (3) (2010) 254–258.

[3] J. S. Walker, Magnetohydrodynamic flows in rectangular ducts with thin conducting walls, Journal de Mécanique 20 (1) (1981) 79–112.

[4] L. Bühler, Magnetohydrodynamic flows in arbitrary geometries in strong, nonuniform magnetic fields, Fusion Technology 27 (1995) 3–24.

[5] C. Mistrangelo, L. Bühler, Development of a numerical tool to simulate magnetohydrodynamic interactions of liquid metals with strong applied magnetic fields, Fusion Science and Technology 60 (2) (2011) 798–803.

[6] L. Bühler, A parametric study of 3D MHD flows in expansions of rectangular ducts, Fusion Science and Technology 52 (3) (2007) 595–602.

[7] C. Mistrangelo, Topological analysis of separation phenomena in liquid metal flow in sudden expansions. Part II: Magnetohydrodynamic flow, Journal of Fluid Mechanics 674 (2011) 132–162.

[8] C. Mistrangelo, L. Bühler, Magnetohydrodynamic pressure drops in geometric elements forming a HCLL blanket mock-up, Fusion Engineering and Design 86 (2011) 2304–2307.